

Isostaticity of Constraints in Jammed Systems of Soft Frictionless Platonic Solids

Kyle C. Smith and Timothy S. Fisher

*Birck Nanotechnology Center and School of Mechanical Engineering,
Purdue University, West Lafayette, Indiana 47906, USA*

Meheboob Alam

*Engineering Mechanics Unit,
Jawaharlal Nehru Centre for Advanced Scientific Research,
Jakkur P.O., Bangalore 560064, India*

We show that the average number of constraints per particle $\langle C_{total} \rangle$ in mechanically stable disordered systems of Platonic solids (except cubes) approach the isostatic limit at the jamming point ($\langle C_{total} \rangle \rightarrow 12$), even though all Platonic solids are hypostatic according to the average number of contacts. By introducing angular alignment metrics to classify the degree of constraint imposed by each contact, we find that constraints arise as a direct result of local orientational order that locally breaks continuous symmetry in face-face alignment angle distributions, with approximately one face-face contact per particle at jamming. In contrast, the cubically-ordered system of cubes exhibits an abundance of hyper-acute face-face alignment angles with vanishing higher-order mechanical constraint that is responsible for hyperstatic constraints in that system ($\langle C_{total} \rangle > 12$).

PACS numbers: 45.70.Cc, 45.50.-j, 61.43.-j

Maxwell [1] analyzed the mechanical stability of soft structural frames by considering that a given force imparts only one constraint on a structure's motion. Following Maxwell's approach, jammed assemblies of frictionless spheres exhibit average number of contacts per particle $\langle Z_{total} \rangle$ equal to the isostatic value $2n_f$ [2], where n_f is the degrees of freedom per particle. In contrast, ellipses [3–5], ellipsoids [4, 5], tetrahedra [6, 7], and the remaining Platonic solids [7] [Fig.1(a)] exhibit hypostatic behavior ($\langle Z_{total} \rangle < 2n_f$). The isostatic condition has been linked to the mechanical stability of soft sphere systems [8], and the hypostaticity of ellipses has been attributed to the presence of floppy vibrational modes, which provide vanishing restoring force [3]. Jaoshvili *et al.* [6] recently showed that the average constraint number $\langle C_{total} \rangle$, which incorporates topology-dependent contact constraint (e.g., through vertex-face, edge-edge, edge-face, and face-face contact topologies), is isostatic for tetrahedral dice even though $\langle Z_{total} \rangle < 2n_f$. Similar approaches incorporating variable contact constraint have been utilized in the prediction of mechanism mobility as early as 1890 (see [9]). The presupposition underlying constraint counting is the mechanical independence of constraints. As a result, such constraint counting approaches fail to predict the true mobility of mechanisms when kinematic redundancy is present (see [9]), and therefore such approaches are not guaranteed to predict $\langle C_{total} \rangle$ at the jamming point. The dependence of $\langle Z_{total} \rangle$ on sphericity of the Platonic solids suggests that the distributions of face-face, edge-face, and lower order (e.g., vertex-face and edge-edge) contact topologies depend on particle shape [7], and are therefore appropriate candidates for the study of constraint counting for arbitrarily-shaped faceted particles. One goal of the

present work is to check the validity of generalized isostaticity constraint [6] for all Platonic solids.

Additionally, packing density and structure of Platonic solids have been the focus of recent studies. All Platonic solids except for tetrahedra pack optimally in Bravais lattices [10]. In contrast, tetrahedra pack optimally in a highly ordered double-dimer configuration [11–13]. Random close packed tetrahedral dice [6, 14], athermally jammed tetrahedra [7], and tetrahedroids [15] have exhibited dramatically lower densities [6, 7, 14] and only short-range translational order [6, 7]. Numerous studies have been performed on systems of cube-like particles exhibiting cubatic order [16–19].

The present work investigates the athermal jamming of soft frictionless Platonic solids through energy-based structural optimization. We present jamming threshold density and show that these packings are *vibrationally stable*. The ill-conditioned vibrational spectrum is a direct result of topological heterogeneity in the contact network, and we therefore identify and highlight the orientational order of contacts by introducing angular alignment metrics. Topology classification via angular alignment metric distributions is thereby used in a manner consistent with soft mechanics to assess the *isostaticity of constraints* for all Platonic solids.

Contact model and jamming protocol. Structural optimization coupled with controlled consolidative and expansive strain is used to probe the jamming point as in [7]. The conservative model employed assumes that contact between particles α and β results in energy $E_{\alpha\beta} = YV^2/4V_p$ after a Hookian contact model applied to uniaxially compressed bars, where V is the intersection volume between the particles, V_p is the volume of a single particle, and Y is the elastic modulus. Conjugate

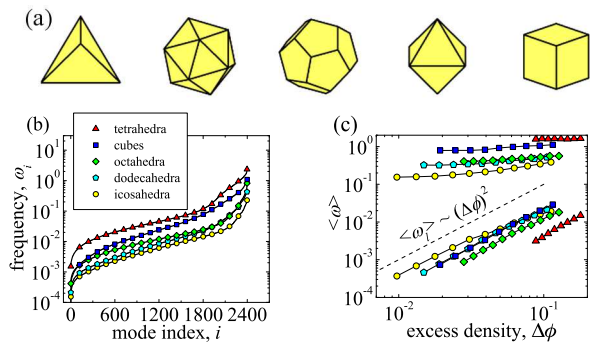


FIG. 1: (Color online) (a) From left to right: tetrahedron, icosahedron, dodecahedron, octahedron, and cube. (b) Vibrational spectra for assemblies nearest the jamming threshold. (c) The power law scaling of $\langle\omega_l\rangle$ (lower curve set) and the asymptotically constant scaling of $\langle\omega_h\rangle$ (upper curve set).

gradient minimization with line searching is utilized with a relative energy change convergence tolerance less than 10^{-12} at each strain step to simulate static equilibrium (see [7]). Density is defined as $\phi = NV_p/V_{cell}$, where V_{cell} and N are the volume and the number of particles of the primary periodic cell.

TABLE I: Jamming threshold ϕ_J estimated for each periodic assembly with 95 % confidence intervals. Experimental values are for mechanically shaken plastic dice with rounded edges [14].

	$N = 100$	$N = 400$	Exp. [14]
Tetrahedra	0.629 ± 0.001	0.634 ± 0.011	0.64 ± 0.01
Octahedra	0.6796 ± 0.0003	0.686 ± 0.001	0.64 ± 0.01
Icosahedra	0.6953 ± 0.0003	0.7008 ± 0.0003	0.59 ± 0.01
Dodecahedra	0.7065 ± 0.0002	0.7085 ± 0.0003	0.63 ± 0.01
Cubes	0.794 ± 0.002	0.791 ± 0.001	0.67 ± 0.02

Assemblies of monodisperse Platonic solids with periodic cubic lattice boundary conditions were consolidated with average energy per particle near $3.2 \times 10^{-5} YV_p$ from low-density random configurations at $\phi = 0.05$. Estimates of the jamming threshold density ϕ_J were obtained by expansion toward the jamming point as in [7] (see Table I). ϕ_J converges well at $N = 100$, but the results differ somewhat from the ‘random close packed’ densities measured by [14] for finite systems of rounded dice. Unless otherwise stated, hereafter the results presented are for $N = 400$.

Mechanical stability. We computed the low-energy vibrational spectra of these monodisperse systems as $\omega_i = \sqrt{\lambda_i/m}$ (as in [3]), where λ_i is the i^{th} eigenvalue of the dynamical matrix $D_{\alpha\beta} = \partial^2 E / \partial \mathbf{r}_\alpha \partial \mathbf{r}_\beta$ and m is particle mass. Frequency ω_i is presented in units of $V_p^{1/3} \sqrt{Y/\rho}$, where ρ is mass density of the solid phase. Coordinates \mathbf{r}_α of particle α are composed of translational $x_{i,\alpha}$ and rotational $\theta_{i,\alpha}$ components $\mathbf{r}_\alpha = \{x_{1,\alpha}, x_{2,\alpha}, x_{3,\alpha}, R_\alpha \theta_{1,\alpha}, R_\alpha \theta_{2,\alpha}, R_\alpha \theta_{3,\alpha}\}$, where R_α is the radius of gyration (see [20]). We calcu-

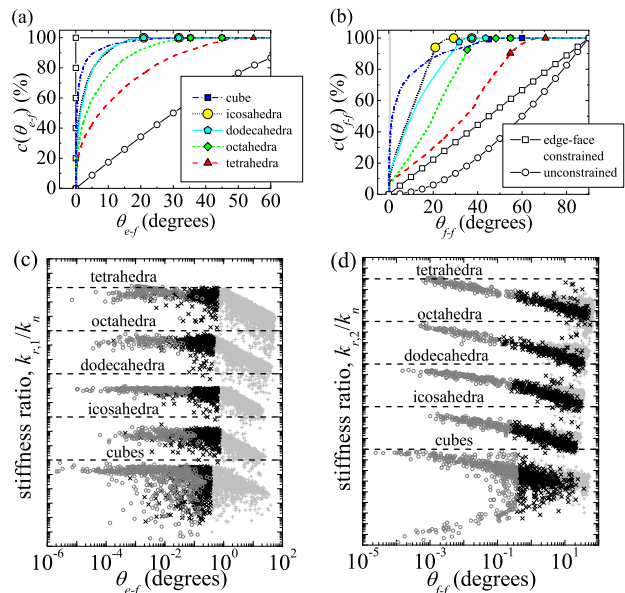


FIG. 2: (Color online) CDFs of (a) θ_{e-f} and (b) θ_{f-f} . Points plotted on the simulated curves correspond to $c(\theta_{e-f,c,i})$ and $c(\theta_{f-f,c,i})$. Region 1 of $c(\theta_{f-f})$ is masked in gray, while region 2 extends from the edge of region 1 to $\theta_{f-f,c,min}$, the minimum critical face-face alignment angle. Ideal random CDFs for edge-face constrained (open squares) and unconstrained (open circles) contacts are displayed as well. (c) First rotational stiffness ratio versus θ_{e-f} and (d) second rotational stiffness ratio versus θ_{f-f} . Gray circles, black crosses, and light gray plus signs represent face-face, edge-face, and lower order contacts, respectively.

late $D_{\alpha\beta}$ through central differences of forces and moments, considering only its symmetric part. The resulting spectra of systems with density nearest ϕ_J are displayed in Fig.1(b). At all densities we find $6N - 3$ stable modes with 3 trivial (rigid body) translational modes, confirming that our soft packings are indeed stably jammed as in [3, 8]. This result also confirms that all N particles participate in the mechanical network, and therefore no rattlers exist. The mean values of the 50 lowest and highest non-trivial frequency modes $\langle\omega_l\rangle$ and $\langle\omega_h\rangle$ were computed and plotted against excess density, $\Delta\phi = \phi - \phi_J$ [Fig.1(c)]. The scaling of $\langle\omega_l\rangle$ with respect to $\Delta\phi$, $\langle\omega_l\rangle \sim (\Delta\phi)^2$, reveals that these packings are in fact marginally stable at the jamming point, while finite $\langle\omega_h\rangle$ persists at the jamming point [Fig.1(c)], as a result of stiff face-face contacts. Energies of these systems scale as $E \propto (\Delta\phi)^6$ [7] with bulk modulus K scaling as $K \propto (\Delta\phi)^4$. Therefore it is clear that low frequency modes are excited by volumetric strain because $\langle\omega_l\rangle \propto \sqrt{K} \propto (\Delta\phi)^2$.

Angular alignment. Soft contacts between faceted particles can be classified as face-face, edge-face, or lower order. Accordingly we define angular order metrics that approach zero as contacts orient with perfect face-face or

edge-face alignment; these metrics could be measured experimentally with tomographic reconstruction. The face-face alignment angle $\theta_{f-f,ql}$ of contacting particles q and l is expressed as $\theta_{f-f,ql} = \pi - \cos^{-1}(\min(\hat{n}_{qi}^T \hat{n}_{lj}))$, where \hat{n}_{qi} is the normal vector of face i on particle q . The minimum is computed over all combinations of i and j corresponding to intersecting faces on the respective particles. The edge-face alignment angle θ_{e-f} is calculated as the minimum of $\theta_{e-f,ql}$ and $\theta_{e-f,lq}$, where $\theta_{e-f,ql} = \sin^{-1}(\min(|\hat{e}_{qi}^T \hat{n}_{lj}|))$, and \hat{e}_{qi} is the unit edge vector of edge i on particle q .

Randomly oriented faces and edges provide a starting point for understanding the distribution of alignment angles in jammed assemblies. Three-dimensional (3D) random edges and faces possess probability density of edge-face alignment with $p(\theta_{e-f}) \propto \cos(\theta_{e-f})$. The occurrence of edge-face contacts is therefore expected to be ubiquitous in jammed assemblies, because probability is weighted toward small θ_{e-f} . In contrast, face-face contacts are expected to be less common, because 3D random faces possess alignment probability density that vanishes in the face-face limit ($p(\theta_{f-f}) \propto \sin(\theta_{f-f})$). On the other hand, $p(\theta_{f-f})$ for edge-face constrained contacts exhibit uniform probability. Thus, face-face contacts are only expected to occur through edge-face constrained rotations.

Cumulative distribution functions (CDFs) are plotted in Figs.2(a-b) for all the contacts in one realization of each system in addition to CDFs of ideal random systems. Plotted points correspond to critical alignment angles $\theta_{e-f,c,i}$ and $\theta_{f-f,c,i}$ for topology i (see [21]). The edge-face alignment CDF $c(\theta_{e-f})$ of each system in Fig.2(a) is heavily weighted toward small angles more so than for ideal random systems. With the exception of cubes, the angular breadth of a given distribution spans proportional to $\theta_{e-f,c,min}$, the minimum critical alignment angle among vertex-face and edge-edge contacts. This results in particles with large $\theta_{e-f,c,min}$ having less probability of near edge-face contacts. Despite this deviation all Platonic solids have hyper-random probability at small θ_{e-f} (see [21]) with CDF approaching that of edge-face constrained contacts [open squares, Fig.2(a)].

Fig.2(b) shows that $c(\theta_{f-f})$ for all Platonic solids (except cubes) possess three regions of descending probability density: (1) ultra-low angle ($< 1^\circ$) face-face contact region, (2) intermediate uniform probability region, and (3) high angle region. Region 2 contains the largest portion of total contacts and exhibits $c(\theta_{f-f})$ similar to that of random edge-face constrained contacts [open squares, Fig.2(b)], rather than unconstrained contacts [open circles, Fig.2(b)]. This is a direct result of the abundance of contacts with small θ_{e-f} that exhibit CDFs approaching that of edge-face constrained contacts [open squares, Fig.2(a)], rather than unconstrained contacts [open circles, Fig.2(a)]. In a sense, region 2 possesses continuous rotational symmetry (*i.e.*, angle invariant $p(\theta_{f-f})$)

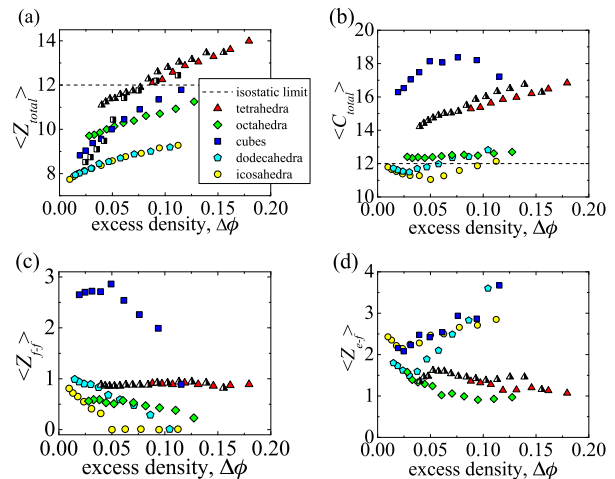


FIG. 3: (Color online) Variation of average (a) contact, (b) constraint, (c) face-face contact, and (d) edge-face contact number with $\Delta\phi$. Half-filled symbols represent data for systems of $N = 100$, while the remainder are for $N = 400$.

resulting in increased probability for contacts to form with acute θ_{f-f} [Fig.2(b)], relative to completely unconstrained random systems [open circles, Fig.2(b)]. Kinematic interactions in region 1 [gray mask, Fig.2(b)] produce local breaking of continuous symmetry through face-face contacts, acting as ordered inclusions in orientationally disordered systems. This non-ergodic effective phase space reduction is similar to that observed in systems of hard ellipsoids where local hypostaticity results from concerted orientational ordering [22].

Cubes on the other hand exhibit continuously decreasing probability density away from $\theta_{f-f} = 0$, which is a direct result of the *cubic phase* (see [21]). We find that the nematic order parameter does not increase as the jamming point is approached (see [21]), and therefore the persistence of imperfect cubaticity as the jamming point is approached results in contacts with persistently small, but non-zero θ_{f-f} .

Constraint isotaticity and topological distributions. To classify topologies we fit $c(\theta_{e-f})$ and $c(\theta_{f-f})$ independently with a piecewise continuous distribution function basis $c_f(\theta) = H(\theta - \alpha) \sum_{i=0}^n a_i \theta^i$, where n is polynomial order, a_i are fitted coefficients, H is the Heaviside step function, and α is fitted CDF discontinuity. We determine angular alignment cutoffs for topological classification θ_{cut} satisfying $c_f(\alpha) = c(\theta_{cut})$. We classify edge-face contacts as those with $\theta_{e-f} < \theta_{e-f,cut}$ and $\theta_{f-f} \geq \theta_{f-f,cut}$ and face-face contacts as those with $\theta_{f-f} < \theta_{f-f,cut}$.

Because most $c(\theta_{f-f})$ exhibit linear behavior at small θ_{f-f} in region 2, we choose $n = 1$ and confine the fit to $\theta_{f-f} < 5^\circ$. Scaling of $c(\theta_{e-f})$ in the lower order contact regime ($\theta_{e-f} \geq \theta_{e-f,cut}$) is less obvious, so we find the value of n yielding highest consistency with mechanical

metrics (see [21]). The CDF of cubes exhibits features uncommon to other systems, and as a result alternative fitting parameters were employed for that system (see [21]). We estimate normal stiffness k_n , first rotational stiffness $k_{r,1}$, and secondary rotational stiffness $k_{r,2}$ to assess the mechanical consistency of constraints imposed by each contact; detailed descriptions of these parameters are included in [21]. Scatter plots of stiffness ratios ($k_{r,1}/k_n$ and $k_{r,2}/k_n$) versus relevant alignment angles are displayed in Fig.2(c-d). $k_{r,1}/k_n$ are large for face-face and edge-face topologies, while $k_{r,2}/k_n$ are large only for face-face topologies. We confirm that all Platonic solids (except cubes) exhibit large $k_{r,1}/k_n$ for small θ_{e-f} and large $k_{r,2}/k_n$ for small θ_{f-f} . Cubes exhibit much less correlation between these parameters. For example, an abundance of contacts have small $k_{r,1}/k_n$ and $k_{r,2}/k_n$ at small values of θ_{e-f} and θ_{f-f} , respectively [lowest panels in Fig.2(c-d)]. This observation is contrary to the presupposition underlying kinematic constraint counting that aligned contacts produce higher-order rotational constraint. This is an indirect evidence that $\langle C_{total} \rangle$ (see below) is *hyperstatic* for cubes.

The variation of average contact number $\langle Z_{total} \rangle$ with respect to $\Delta\phi$ [Fig.3(a)] confirms the generally hypostatic nature of $\langle Z_{total} \rangle$, consistent with our previous findings for smaller systems [7]. $\langle Z_{total} \rangle$ versus $\Delta\phi$ is independent of system size with the exception of cubes, as displayed in Fig.3(a). $N = 400$ cubes exhibits smoother variation of $\langle Z_{total} \rangle$ than $N = 100$, because it exhibits an isotropic cubatic phase in contrast to the anisotropic nematic phase formed by $N = 100$ (see [21]).

We determine the average contact number for face-face $\langle Z_{f-f} \rangle$, edge-face $\langle Z_{e-f} \rangle$, and lower order (*i.e.*, vertex-face and edge-edge) contacts $\langle Z_l \rangle$. The average constraint number $\langle C_{total} \rangle$ is thereby calculated as $\langle C_{total} \rangle = 3\langle Z_{f-f} \rangle + 2\langle Z_{e-f} \rangle + \langle Z_l \rangle$ [6]. Importantly, $\langle C_{total} \rangle$ of all Platonic solids (except cubes) approaches values near the isostatic limit [Fig.3(b)], in contrast with $\langle Z_{total} \rangle$ [Fig.3(a)]. Thus, these highly disordered systems possess contacts which independently constrain motion, in contrast to the dependent constraints in the system of cubes. The contributions of each topology to $\langle C_{total} \rangle$ is displayed in Fig.3(c-d). At large $\Delta\phi$, cubes, dodecahedra, icosahedra, and octahedra exhibit low $\langle Z_{f-f} \rangle$, increasing as $\Delta\phi \rightarrow 0$ [Fig.3(c)]. Tetrahedra exhibit nearly constant $\langle Z_{f-f} \rangle$. Disordered systems of Platonic solids possess $\langle Z_{f-f} \rangle \lesssim 1$. We attribute this effect to a two-fold rotational constraint induced on a given particle once a single face-face contact is formed. Such a rotational constraint appears to hinder the formation of additional face-face contacts. Octahedra exhibit diminished $\langle Z_{f-f} \rangle$ as a result of weak nematicity (see [21]). Only for highly ordered systems that exhibit collective and concerted rearrangements can more face-face contacts form, as exhibited by cubes [Fig.3(c)]. Note that low $\langle Z_{f-f} \rangle$ of tetrahedra is in striking contrast with values of 2-3 face-face

contacts recently reported for tetrahedral dice [6].

These results also suggest that $\langle Z_{f-f} \rangle$ or a convolution of $p(\theta_{f-f})$ are suitable order parameters that can be used to determine the *maximally random jammed* state of assemblies of faceted particles according to the approach described in [23]. Comparison of the random packings studied here with $\langle Z_{f-f} \rangle$ for the optimal Bravais lattices of Platonic solids (see [10]) reveals that optimal packing is entropically frustrated, as a result of higher $\langle Z_{f-f} \rangle$ compared to the systems investigated here.

In summary, we have established the *isostaticity of constraints* in disordered jammed systems of Platonic solids (*i.e.* all except cubes) and have linked this condition to their *mechanical stability*. The near unity jamming face-face contact number exhibited by all Platonic solids (except cubes) should motivate further study into the finite extent of face-face clusters. The percolation of heat and electricity through such clusters could be exploited to tailor effective transport properties of granular materials for energy applications (*e.g.*, thermoelectric devices, lithium ion batteries, and solid-state hydrogen storage). Additionally, the hyperstatic behavior of ordered systems, as observed for cubes, is a rich subject for future study.

Acknowledgments. The authors acknowledge the Indo-U.S. Science and Technology Forum for supporting Purdue-JNCASR exchanges through the Joint Networked Centre on Nanomaterials for Energy (Award No. 115-2008/2009-10) and the U.S. National Science Foundation for workshop support (Grant No. OISE-0808979) and graduate research support to K.C.S. K.C.S. also thanks the Purdue Graduate School for financial support. We also thank Bruce Craig and Wen Wei Loh of the Statistical Consulting Service at Purdue for helpful discussions.

-
- [1] J. C. Maxwell, Phil. Mag. **27**, 294 (1864).
 - [2] C. F. Moukarzel, Phys. Rev. Lett. **81**, 1634 (1998).
 - [3] M. Mailman, C. F. Schreck, C. S. O'Hern, and B. Chakraborty, Phys. Rev. Lett. **102**, 255501 (2009).
 - [4] A. Donev, R. Connelly, F. H. Stillinger, and S. Torquato, Phys. Rev. E **75**, 051304 (2007).
 - [5] A. Donev, I. Cisse, D. Sachs, E. A. Variano, F. H. Stillinger, R. Connelly, S. Torquato, and P. M. Chaikin, Science **303**, 990 (2004).
 - [6] A. Jaoshvili, A. Esakia, M. Porrati, and P. M. Chaikin, Phys. Rev. Lett. **104**, 185501 (2010).
 - [7] K. C. Smith, M. Alam, and T. S. Fisher, Phys. Rev. E **82**, 051304 (2010).
 - [8] C. S. O'Hern, L. E. Silbert, A. J. Liu, and S. R. Nagel, Phys. Rev. E **68**, 011306 (2003).
 - [9] G. Gogu, Mech. Mach. Theory **40**, 1068 (2005).
 - [10] S. Torquato and Y. Jiao, Nature **460**, 876 (2009).
 - [11] Y. Kallus, V. Elser, and S. Gravel, Dis. and Comp. Geom. **44**, 245 (2010).

- [12] E. Chen, M. Engel, and S. Glotzer, *Dis. and Comp. Geom.* **44**, 253 (2010).
- [13] S. Torquato and Y. Jiao, *Phys. Rev. E* **81**, 041310 (2010).
- [14] J. Baker and A. Kudrolli, *Phys. Rev. E* **82**, 061304 (2010).
- [15] L. Shui-Xiang, Z. Jian, and Z. Xuan, *Chin. Phys. Lett.* **25**, 1724 (2008).
- [16] B. S. John, A. Stroock, and F. A. Escobedo, *J. Chem. Phys.* **120**, 9383 (2004).
- [17] G. W. Delaney and P. W. Cleary, *EPL* **89**, 34002 (2010).
- [18] Y. Jiao, F. H. Stillinger, and S. Torquato, *Phys. Rev. E* **81**, 041304 (2010).
- [19] R. D. Batten, F. H. Stillinger, and S. Torquato, *Phys. Rev. E* **81**, 061105 (2010).
- [20] J. Satterly, *The Mathematical Gazette* **42**, 11 (1958).
- [21] K. C. Smith, M. Alam, and T. S. Fisher, *Supplementary information available as a separate pdf file* (2011).
- [22] P. M. Chaikin, A. Donev, W. Man, F. H. Stillinger, and S. Torquato, *Ind. Eng. Chem. Res.* **45**, 6960 (2006).
- [23] S. Torquato, T. M. Truskett, and P. G. Debenedetti, *Phys. Rev. Lett.* **84**, 2064 (2000).